Control of ciliary transcriptional programs during spermatogenesis by antagonistic transcription factors

Weihua Wang[1,4]✉, Junqiao Xing[1,4], Xiqi Zhang[2,4], Hongni Liu[1], Haochen Jiang[1], Cheng Xu[1], Xue Zhao[1], Zhangfeng Hu[1,2,3]✉

[1]Hubei Key Laboratory of Cognitive and Affective Disorders, Wuhan Institute of Biomedical Sciences, School of Medicine, Jianghan University, Wuhan, 430056 Hubei, China

[2]School of Life Sciences, Jianghan University, Wuhan, 430056 Hubei, China

[3]Hubei Key Laboratory of Environmental and Health Effects of Persistent Toxic Substances, Jianghan University, Wuhan, 430056 Hubei, China

[4]These authors contributed equally: Weihua Wang, Junqiao Xing, Xiqi Zhang

✉e-mail: wangwh2019@163.com; huzhangfenghzf@163.com

Abstract

Existence of cilia in the last eukaryotic common ancestor (LECA) raises a fundamental question in biology: how the transcriptional regulation of ciliogenesis has evolved? One conceptual answer to this question is by an ancient transcription factor regulating ciliary gene expression in both unicellular and multicellular organisms, but examples of such transcription factors in eukaryotes are lacking. Previously, we showed that an ancient transcription factor XAP5 is required for flagellar assembly in *Chlamydomonas*. Here, we show that XAP5 and XAP5L are two conserved pairs of antagonistic transcription regulators that control ciliary transcriptional programs during spermatogenesis. Male mice lacking either XAP5 or XAP5L display infertility, as a result of meiotic prophase arrest and sperm flagella malformation, respectively. Mechanistically, XAP5 positively regulates the ciliary gene expression by activating the key regulators including FOXJ1 and RFX families during the early stage of spermatogenesis. In contrast, XAP5L negatively regulates the expression of ciliary genes via repressing these ciliary transcription factors during the spermiogenesis stage. Our results provide new insights into the mechanisms by which temporal and spatial transcription regulators are coordinated to control ciliary transcriptional programs during spermatogenesis.

Introduction

Cilia and flagella are evolutionarily conserved hair-like microtubule organelles that project from the surfaces of most eukaryotic cells(Derderian, Canales, & Reiter, 2023; Mitchell, 2017). They play essential roles in sensory reception, signal transduction and cell movement(Goetz & Anderson, 2010; Nachury & Mick, 2019; Singla & Reiter, 2006). The dysfunction of cilia in humans leads to an emerging class of genetic diseases called ciliopathies classified into first-order and second-order ciliopathies(Ishikawa & Marshall, 2011; Lovera & Lüders, 2021; Reiter & Leroux, 2017). First-order ciliopathies are caused by aberrations in ciliary proteins, and second-order ciliopathies occur due to defects in non-ciliary proteins, such as transcription factors, that are required for cilia formation and function(Reiter & Leroux, 2017).

Cilia are complex organelles and are dynamically regulated during development and the cell cycle(Eggenschwiler & Anderson, 2007; Kasahara & Inagaki, 2021; Santos & Reiter, 2008). The transcriptional regulation of ciliary genes must be precisely coordinated during ciliogenesis(Choksi, Lauter, Swoboda, & Roy, 2014; Collins, Ventrella, & Mitchell, 2021; Lewis & Stracker, 2021; Thomas et al., 2010). In metazoans, several transcription factors, including FOXJ1 and RFXs, have been shown to be involved in directing the expression of ciliary genes(Stubbs, Oishi, Izpisua Belmonte, & Kintner, 2008; Swoboda, Adler, & Thomas, 2000; Yu, Ng, Habacher, & Roy, 2008). These key ciliary transcription factors show dynamic expression patterns during development and differentiation(Stubbs et al., 2008; Swoboda et al., 2000; Yu et al., 2008). However, how these key transcriptional

programs are spatially and temporally controlled by cell type-specific transcription factors and signaling pathways in order to activate specific target ciliary genes and generate diverse cilia is largely unknown.

Despite transcriptional regulation of ciliary genes is required for ciliogenesis in both unicellular and multicellular organisms, the underlying mechanism mediating ciliary gene expression may be fundamentally different, as the two major transcription factors, FOXJ1 and RFXs, are absent from many unicellular organisms(Chu, Baillie, & Chen, 2010; Li et al., 2018; Piasecki, Burghoorn, & Swoboda, 2010; Vij et al., 2012). Cilia and ciliary genes have been highly conserved throughout evolution, suggesting that the regulation of ciliary genes could be programmed by yet undiscovered transcriptional mechanisms, which possibly coevolved with multicellularity. Recently, an ancient transcription factor, XAP5, is found to regulate ciliary gene expression in a unicellular organism, *Chlamydomonas reinhardtii*(Li et al., 2018). XAP5 is highly conserved among different species and is widely expressed across tissues(Martin-Tryon & Harmer, 2008; Mazzarella, Pengue, Yoon, Jones, & Schlessinger, 1997). In vertebrates, *XAP5-like* (*XAP5L*) with an intronless open reading frame originated in Therians via retrotransposition of the ancestral *XAP5*, and it is highly expressed during spermatogenesis(Sedlacek et al., 1999; A. Zhang et al., 2011). However, whether XAP5 and XAP5L play essential roles in cilia development in multicellular organisms remains unknown.

Here, we show that XAP5/XAP5L are antagonistic transcription factors required for ciliary transcriptional programs during spermatogenesis. XAP5 is widely expressed in

different tissues, while XAP5L is exclusively present in the testes. To explore the roles of XAP5/XAP5L in ciliogenesis, we generated a *XAP5L* knockout (KO) mouse line and found that *XAP5L* KO male mice are infertile due to the malformation of sperm flagella. Interestingly, male mice with the loss of XAP5 protein in germ cells also exhibited infertile, due to the arrest of spermatogenesis in the meiotic prophase stage. These data suggest that XAP5/XAP5L play crucial roles in sperm flagellar assembly. Mechanistically, XAP5 positively modulates transcriptional rewiring of ciliary genes via activating the key regulators including FOXJ1 and RFXs during the early stage of spermatogenesis. Conversely, XAP5L negatively regulates the transcriptional program controlling ciliogenesis by repressing these ciliary transcription factors during the spermiogenesis stage. Thus, ciliary transcriptional programs are spatially and temporally controlled by XAP5/XAP5L antagonistic transcription factors during spermatogenesis.

Results

XAP5 and XAP5L are indispensable for male fertility

To explore the potential functions of XAP5/XAP5L during ciliogenesis *in vivo*, we performed Western blot analysis to investigate the spatiotemporal expression of XAP5/XAP5L in various mouse tissues. We observed that XAP5 protein was widely expressed in diverse tissues and present at all stages of postnatal testes maturation, whereas XAP5L protein was mainly present in the testes and its level increased dramatically from postnatal day 21 (P21) and continued into adulthood (Figures 1A, B). Next, we identified

the specific testicular cell types expressing XAP5/XAP5L using published single-cell RNA-seq data(Jung et al., 2019). XAP5 mRNA was found predominantly expressed in spermatogonia, while XAP5L mRNA was observed in pachytene spermatocytes, and remained until elongating spermatids (Figure 1C). Consistent with the mRNA localization patterns, immunofluorescence staining showed that XAP5 protein was mainly detected in the nuclei of spermatogonia, whereas XAP5L protein was present in the nuclei of pachytene spermatocytes and spermatids within the seminiferous tubules, and neither of XAP5 or XAP5L was detected in mature sperm (Figure 1D and Figure S1).

To investigate the physiological function of the uncharacterized XAP5/XAP5L protein, we attempted to generate global KO mice using the CRISPR-Cas9 system. We successfully established a *XAP5L* KO mouse line (Figures S2A-C) and found that while all *XAP5L* KO mice survived to adulthood and appeared indistinguishable from the wildtype (WT) mice, *XAP5L* KO males were sterile (Figures 1E, F). Notably, generating mosaic F0 founders with *XAP5* mutant allele proved challenging, and no F1 generation inherited the mutant alleles from the few F0 founders in over a year of breeding experiments, underscoring the critical roles of XAP5 in mouse development. Subsequently, we generated floxed-*XAP5* mice and crossed them with *Stra8-GFPCre* knockin mice(Lin et al., 2017) to produce *XAP5* germline-specific KO mice (*XAP5* cKO) (Figures S2D-F). Similar in appearance to controls ($XAP5^{fl/Y}$), all *XAP5* cKO males were also found to be sterile (Figures 1G, H). Collectively, these results suggest that XAP5/XAP5L play essential roles in spermatogenesis.

XAP5 and XAP5L function at different stages of spermatogenesis

To uncover the cause of male infertility, we conducted gross and histological analyses of the testes from WT and *XAP5L* KO mice. There were no differences in the gross appearance of testis or in the weight of mouse body and testis between WT and XAP5L KO mice (Figure 2A). Histological analysis did not reveal any severe abnormity in the seminiferous epithelial cycle of XAP5L KO testes (Figure 2B). We then investigated the motility of sperm collected from cauda epididymis, and found that total motility of sperm was significantly reduced in *XAP5L* KO mice (Figure 2C and Videos S1, 2). Further examination of the morphology and structure of cauda epididymal sperm in *XAP5L* KO mice revealed significantly higher rates of abnormal flagella (Figures 2D-F), indicating that XAP5L is crucial for flagellar assembly during spermiogenesis.

We also investigated the spermatogenic defects in the seminiferous tubules and epididymis of *XAP5* cKO male mice. Notably, the testes of *XAP5* cKO males were significantly smaller compared to WT controls at P16 and older (Figure 3A). Many seminiferous tubules in P16 and older *XAP5* cKO males were vacuolated due to the absence of spermatocytes and spermatids, as indicated by the lack of XY body formation and the absence of PNA signal, a marker of spermatids and sperm, in *XAP5* cKO germ cells (Figures 3B-D). As a consequence, no sperm were observed in the adult cauda epididymides of *XAP5* cKO mice (Figure 3E). Taken together, these data indicate that germ cell development in *XAP5* cKO males was arrested in meiotic prophase, and XAP5 is indispensable for meiotic progression during spermatogenesis.

XAP5 and XAP5L function as antagonistic regulators of ciliary transcriptional regulatory networks via regulating transcription factors

To gain insight into the regulatory mechanisms of XAP5L during sperm flagellar assembly, we employed RNA-seq analysis to examine mature sperm collected from the cauda epididymis of WT and *XAP5L* KO adult mice. Differential expression analysis identified 2093 upregulated and 267 downregulated genes in *XAP5L* KO sperm (Figure S3A). Gene ontology analysis revealed that the upregulated genes were associated with cilia assembly or function (Figure 4A and Figures S3B, C). When crossed with the previously compiled ciliogenesis-related gene list(Nemajerova et al., 2016), the upregulated genes were observed encompassing diverse structural and functional components of the ciliogenic program (Table S1 and Figure S3D). Notably, several key transcription factor (TF) regulators of ciliogenesis were among the upregulated genes, including FOXJ1 and RFX families (Figures 4B, C and Figure S3E). Moreover, several key regulators of spermatogenesis, particularly spermiogenesis, were identified, including RFX2(Kistler et al., 2015; Wu et al., 2016), SOX families(Schartl et al., 2018; D. Zhang et al., 2018), TAF7L(Zhou et al., 2013) and TBPL1(Martianov et al., 2001) (Figure 4B and Figure S3E). Many core ciliary genes were also upregulated, such as *CFAP206*(Beckers et al., 2020) and *IFT81*(Qu et al., 2020) which are critical for male fertility (Figure S3E), consistent with the tight coregulation between spermiogenesis and cilia-related genes during spermatogenesis. These findings suggest that the genes identified in our study provide an excellent resource for candidates with novel ciliary or spermatogenesis-related functions,

and the newly identified testes-specific protein TULP2(Oyama et al., 2022; Zheng et al., 2021) was selected for validation. We observed that *TULP2* KO male mice were sterile due to malformation of sperm flagella (Figure S4). Overall, our results clearly indicate that XAP5L acts as a central transcriptional repressor of ciliogenesis during mouse spermatogenesis.

Furthermore, we performed RNA-seq analysis using P16 testes samples from WT and *XAP5* cKO mice to explore the underlying mechanism of XAP5-mediated germ cell loss. Differential expression analysis identified 554 upregulated and 1587 downregulated genes in *XAP5* cKO sperm (Figure S5A). We observed that the downregulated genes in *XAP5* cKO males were involved in cilium assembly or functions (Figure 4D and Figures S5B-D). Strikingly, many of these downregulated genes were upregulated in *XAP5L* KO sperm, including the key ciliogenesis regulators FOXJ1 and RFX families (Figures 4E, F, Figure S5E and Table S1). In addition, meiosis initiation marker STRA8(Anderson et al., 2008; Ferder et al., 2019), meiosis-specific genes SPO11(Romanienko & Camerini-Otero, 2000) and DMC1(Bishop, Park, Xu, & Kleckner, 1992), key transcription regulators of spermiogenesis RFX2(Kistler et al., 2015; Wu et al., 2016), SOX30(D. Zhang et al., 2018) and CREM(Blendy, Kaestner, Weinbauer, Nieschlag, & Schutz, 1996; Nantel et al., 1996) were also downregulated in *XAP5* cKO mice (Figures 4E and S5F), consistent with the aforementioned result that loss of XAP5 induced spermatogenesis arrest in meiotic stage. Considering the evolutionary conservation of XAP5/XAP5L protein across different species and the expression patterns of XAP5, XAP5L, FOXJ1 and RFX factors during

spermatogenesis (Figures 1C and S6), these results suggest that XAP5 and XAP5L have antagonistic effects, and they may function upstream of the transcription factor families, including FOXJ1 and RFX factors, to coordinate the ciliogenesis during spermatogenesis (Figure 4G).

Discussion

Cilia and flagella are ancient organelles present in the last eukaryotic common ancestor (LECA)(Mitchell, 2017). Cilia assembly and maintenance are under strict transcriptional regulation in both unicellular and multicellular organisms(Choksi et al., 2014; Collins et al., 2021; Lewis & Stracker, 2021; Thomas et al., 2010). Despite cilia and flagella having an ancient origin, the evolutionary history of ciliary gene regulation has remained an unsolved problem. The main reason is that the master ciliary transcription factors found in multicellular organisms, including FOXJ1 and RFXs, are absent from unicellular organisms(Choksi et al., 2014; Collins et al., 2021; Lewis & Stracker, 2021; Thomas et al., 2010). Previously, we showed that an ancient transcription factor, XAP5, was required for flagella assembly in the unicellular green algae *Chlamydomonas*(Li et al., 2018). XAP5 proteins are evolutionarily conserved across diverse organisms(Li et al., 2018; Martin-Tryon & Harmer, 2008), which offers the possibility to investigate the conservation of the role of XAP5 in multicellular organisms. In the present study, we report that XAP5 positively regulates transcriptional network of ciliary genes by activating the key regulators including FOXJ1 and RFXs during spermatogenesis.

Cilia are dynamic organelles, and the expression profile of ciliary genes is dynamic during the cell cycle and under certain physiological conditions(Eggenschwiler & Anderson, 2007; Kasahara & Inagaki, 2021; Santos & Reiter, 2008). Cells have developed regulatory mechanisms to generate functional cilia in a temporal and spatial manner(Choksi et al., 2014; Collins et al., 2021; Lewis & Stracker, 2021; Thomas et al., 2010). However, how ciliary transcription factors determine temporal and spatial ciliary transcriptional programs is poorly understood. Sperm flagellar assembly is likewise tightly regulated during a highly complex temporal process named spermatogenesis(Holstein, Schulze, & Davidoff, 2003; Thomas et al., 2010). Several key transcriptional regulators of spermatogenesis, such as FOXJ1 and RFX2, have been identified(Chen, Knowles, Hebert, & Hackett, 1998; Kistler et al., 2015; Wu et al., 2016). The flagellar formation of FOXJ1-null sperm is severely impaired, and the FOXJ1 target genes are required for sperm motility(Beckers et al., 2020; Chen et al., 1998; Weidemann et al., 2016). *RFX2* KO mice are completely sterile and RFX2 regulates the expression of ciliary genes during spermiogenesis(Kistler et al., 2015; Wu et al., 2016). Ciliary transcription factors (FOXJ1 and RFX2) are dynamically regulated during spermatogenesis(Jung et al., 2019). Intriguingly, our results show that XAP5 and XAP5L are two conserved pairs of antagonistic transcription factors that regulate these key transcriptional regulators required for spermatogenesis.

By using Western blot analysis, we found that XAP5 was ubiquitously expressed in all tissues examined, whereas XAP5L expression was restricted to the testes (Fig. 1a).

Interestingly, previous research found that XAP5L was widely expressed in normal tissue via using TCGA expression data(Thompson et al., 2021). Moreover, loss of XAP5/XAP5L perturbs transcriptional programs in cancer cells. At present, as shown by the recent data, we cannot rule out the possibility that XAP5L is dynamically expressed in other tissues during development. Although XAP5 and XAP5L are highly expressed in testes and critical for spermatogenesis, they are not present in mature sperm (Extended Data Fig. 1). Thus, XAP5/XAP5L are not needed for sperm maintenance. Given the dynamic expression of XAP5/XAP5L during spermatogenesis, it will be interesting to identify the key signaling factors that regulate the timely and spatial expression of XAP5 and XAP5L.

A role for XAP5 in human brain development is suggested by the association of X-linked intellectual disability (XLID) with rare *XAP5* missense variants(Lee et al., 2020). However, how defects in XAP5 lead to XLID syndrome is unknown. Although there is as yet no evidence that XAP5 regulates ciliogenesis in any system besides *Chlamydomonas* and mice, the function in cilia could help clarify the unexplained role of *XAP5* mutations in causing XLID. The possibility that XAP5 could be a ciliary transcription factor in humans would add XLID to the growing list of the second-order ciliopathies.

Materials and Methods

Mice

C57BL/6J strains (from Vital River Laboratories, Beijing, China) and *Stra8-GFPCre* knockin mice (from Cyagen Biosciences) were used. Floxed-*XAP5* mice, *XAP5L* and

TULP2 knockout mice were generated on the C57BL/6J background using the CRISPR/Cas9 system. The sgRNA sequences used to target *XAP5*, *XAP5L* and *TULP2* were as follows: *XAP5L*, sgRNA1-GGC TAC CAG AAA CAG GGA CT, sgRNA2-GGG AGT AAG GTC CCC AAA CT; *XAP5*, sgRNA3-CTA CAG GGC ACT TAT TAA TA, sgRNA4-ATA GTA ATT CCC CCG TGC TT; *TULP2*, sgRNA5-TGA CTA ATT AGG CCC GAG AG, sgRNA6-GGT TCT TAG AGA GTC AAC GT. Experimental protocols were approved by the ethics committees of Jianghan University. Mice were maintained in a pathogen-free environment with a room temperature of 23 ± 2 °C under a humidity level of 30-70%. The light was maintained on a 12-hour day/night cycle.

Genome PCR

Mouse genomic DNA was isolated from the tail tip using One Step Mouse Genotyping Kit (Vazyme, PD101), and subjected to PCR with 2 × Taq Plus Master Mix (Vazyme, P212) following the manufacturer's instructions. The PCR products were separated by 2% agarose gel electrophoresis. The primers used are listed in Table S2.

RNA isolation and real-time PCR

Total RNA was isolated using the TRIzol reagent (Invitrogen, 15596018) and then converted to cDNA with HiScript II 1st Strand cDNA Synthesis Kit (Vazyme, R212) following the manufacturer's instructions. Real-time PCR was conducted using ChamQ SYBR qPCR Master Mix (Vazyme, Q311) on an ABI StepOnePlus real-time PCR system

(Applied Biosystems). Expression values were normalized using the ΔΔCt method with *Gapdh* as the internal control. The primer sequences are indicated in Table S2.

Western blot analysis

Cell lysates from mouse tissues were prepared in RIPA buffer (Beyotime, P0013B) containing Protease Inhibitor Cocktail (Roche, 11873580001) and 1mM PMSF. Subcellular lysates of testicular nuclear and cytoplasmic fractions were prepared using Nuclear and Cytoplasmic Protein Extraction Kit (Beyotime, P0027) following the manufacturer's instructions. The protein lysates were subjected to standard immunoblotting analysis. Antibodies used were as follows: anti-β-actin (ABclonal, AC026), anti-XAP5 (Prospertech, HU-412003), anti-XAP5 (Sigma, HPA003585), anti-XAP5L (Prospertech, Hu-412001), anti-LMNB (Proteintech, 66095-1-Ig), anti-GAPDH (ABclonal, AC002), anti-FOXJ1 (D360355, Sangon Biotech), anti-RFX2 (K110716P, Solarbio) and anti-TULP2 (Prospertech, Hu-412002).

Immunofluorescence

Mouse testis were fixed in 4% paraformaldehyde in PBS at 4 °C overnight, dehydrated in gradient ethanol, embedded in paraffin, and sectioned into 5 μm slices. After deparaffinization and rehydration, testis sections were boiled in 1 mM EDTA, pH 8.0 for 15 min using a microwave oven for antigen retrieval, followed by cooling to room temperature. The primary antibodies, including anti-XAP5 (Prospertech, HU-412003,

1:250 dilution), anti-XAP5 (Sigma, HPA003585, 1:250 dilution), anti-XAP5L (Prospertech, Hu-412001, 1:250 dilution), anti-lectin PNA, Alexa Fluor 488 Conjugate (ThermoFisher, L21409, 1:250 dilution), and anti-TULP2 (Prospertech, Hu-412002, 1:250 dilution), were then incubated at 4 °C overnight. Subsequently, the sections were incubated with the secondary antibody donkey anti-rabbit Alexa Fluor Plus 488 (Invitrogen, A32790, 1:500 dilution) for 1 hour and DAPI for 5 minutes at room temperature. Images were collected using a Zeiss Axio Vert A1 microscope.

Histological analysis

Testes and epididymides were fixed in Bouin's solution (sigma, HT10132) overnight at 4 °C, embedded in paraffin and sectioned into 5 μm slices. The sections were then subjected to H&E staining using standard procedures and observed under a Zeiss Axio Vert A1 microscope.

Assessment of sperm motility and morphology

Cauda epididymides were collected from male mice and dissected in 37°C pre-warmed human tubal fluid (HTF) culture medium (EasyCheck, M1130), followed by incubation at 37°C for 15 min to release the sperm. To assess sperm motility, the sperm suspension was observed and recorded under a Leica total internal reflection fluorescence microscope. Motility was defined as any movement of the sperm flagellum during a 10-second observation cycle. After immobilization with 1% paraformaldehyde, sperm morphology

was observed by H&E staining using standard procedures. Images were captured using a Zeiss Axio Vert A1 microscope equipped with a ×100 oil immersion objective. Sperm without staining were also used to assess sperm morphology. For ultrastructural observation, sperm samples were fixed in 3% glutaraldehyde in 0.1M sodium phosphate buffer (pH7.4), and post-fixed with 1% (wt/vol) OsO_4. After dehydration, the samples were placed in propylene oxide and embedded in a mixture of Epon 812 and Araldite. Ultrathin sections obtained by a Leica EM UC7 ultramicrotome were stained with uranyl acetate and lead citrate, then analyzed using a HT7700 TEM (Hitachi).

Fertility test

Each of the adult male mice was mated with two females for 2 months. All the mice used were aged 6-8 weeks. Vaginal plugs were checked every morning, and the number of newborn pups was counted.

Chromosome spreads and immunofluorescence

Testicular chromosome spreads were prepared and immunolabeled as described(Reinholdt, Ashley, Schimenti, & Shima, 2004). The primary antibodies used were as follows: anti-γ H2AX (Millipore, 05-636, 1:300 dilution), anti-SYCP3 (Proteintech, 23024-1-AP, 1:300 dilution). Secondary antibodies used were Alexa Dye (AlexaFluor Plus 488/594) conjugates (ThermoFisher) at 1:500 dilutions. Images were collected with a Zeiss Axio Vert A1 microscope.

RNA-seq analysis

The mature sperm samples from P56 mice and testis samples from P16 mice were washed three time in 1× PBS after harvest. Total RNA was extracted from the samples using the TRIzol reagent (Invitrogen) and purified with the NEBNext Poly(A) mRNA Magnetic Isolation Module (NEB, E7490). The quality of the RNA samples was examined using the Agilent 2100 Bioanalyzer system (Agilent Technologies). Qualified RNA samples were subjected to sequencing library construction using the NEBNext Ultra II RNA Library Prep Kit for Illumina (NEB, E7775). Paired-end (2 × 150 bp) sequencing was carried out on the Illumina NovaSeq6000 platform. The sequencing reads were mapped to the Mus musculus reference genome (GRCm38/mm10) using HISAT2 v2.1.0(Kim, Langmead, & Salzberg, 2015), and StringTie v1.3.3b(Pertea et al., 2015) was applied to assemble the mapped reads. Fragments Per Kilobase of transcript per Million fragments mapped (FPKM) was used to measure the expression level of a gene. Differential expression analysis was processed by DESeq2 v1.12.4(Subramanian et al., 2005), and the significant differentially expressed genes were identified with a fold change >2. Gene Ontology analysis was performed using the DAVID database.

Statistical analysis

Statistical analyses were conducted using GraphPad Prism 8.0.2 software. All data were presented as mean ± SEM. Values of $P < 0.05$ were considered statistically significant.

Statistical significance between two groups was calculated using an unpaired, parametric, two-sided student's t test.

Materials and Data availability

All relevant data for RNA sequencing have been deposited in the Gene Expression Omnibus database under accession code GSE236388.

The authors declare that all the materials and the data supporting the findings of this study are available within the article and its additional files or from the corresponding authors upon reasonable request.

Acknowledgements

This work was supported by the National Key R&D Program of China (grant number: 2020YFA0907400), the National Natural Science Foundation of China (grant number: 32170702 and 82000828) and the Major Special Funding Program for First-class Discipline Construction of Jianghan University (grant number: 2023XKZ021). We thank Yuan He (Research Center for Medicine and Structural Biology, Wuhan University, China) for the assistance during the experimental design of the transmission electron microscope analysis.

Author Contributions

W.W., J.X., X.Z. and Z.H. designed research; W.W., J.X., X.Z., H.L., H.J., C.X. and X.Z.

performed research; W.W. and Z.H. contributed new reagents/analytic tools; W.W., J.X., X.Z. and Z.H. analyzed data; and W.W. and Z.H. wrote the paper.

Competing interests

The authors declare no competing interests.

Additional files

Table S1

The lists of differential expression genes & ciliogenesis-related genes.

Table S2

The lists of primers used in the Genome PCR and real-time PCR.

Video S1

Representative video of living sperm cells from WT mouse.

Video S2

Representative video of living sperm cells from *XAP5L* KO mouse.

References

Anderson, E. L., Baltus, A. E., Roepers-Gajadien, H. L., Hassold, T. J., de Rooij, D. G., van Pelt, A. M., & Page, D. C. (2008). Stra8 and its inducer, retinoic acid, regulate meiotic initiation in both spermatogenesis and oogenesis in mice. *Proc Natl Acad Sci U S A, 105*(39), 14976-14980. doi:10.1073/pnas.0807297105

Beckers, A., Adis, C., Schuster-Gossler, K., Tveriakhina, L., Ott, T., Fuhl, F., . . . Gossler, A. (2020). The FOXJ1 target Cfap206 is required for sperm motility, mucociliary clearance of the airways and brain development. *Development*. doi:10.1242/dev.188052

402 Bishop, D. K., Park, D., Xu, L., & Kleckner, N. (1992). DMC1: a meiosis-specific yeast homolog of E. coli
403 recA required for recombination, synaptonemal complex formation, and cell cycle progression.
404 *Cell, 69*(3), 439-456. doi:10.1016/0092-8674(92)90446-j
405 Blendy, J. A., Kaestner, K. H., Weinbauer, G. F., Nieschlag, E., & Schutz, G. (1996). Severe impairment of
406 spermatogenesis in mice lacking the CREM gene. *Nature, 380*(6570), 162-165.
407 doi:10.1038/380162a0
408 Chen, J., Knowles, H. J., Hebert, J. L., & Hackett, B. P. (1998). Mutation of the mouse hepatocyte nuclear
409 factor/forkhead homologue 4 gene results in an absence of cilia and random left-right
410 asymmetry. *J Clin Invest, 102*(6), 1077-1082. doi:10.1172/JCI4786
411 Choksi, S. P., Lauter, G., Swoboda, P., & Roy, S. (2014). Switching on cilia: transcriptional networks
412 regulating ciliogenesis. *Development, 141*(7), 1427-1441. doi:10.1242/dev.074666
413 Chu, J. S., Baillie, D. L., & Chen, N. (2010). Convergent evolution of RFX transcription factors and ciliary
414 genes predated the origin of metazoans. *BMC Evol Biol, 10*, 130. doi:10.1186/1471-2148-10-
415 130
416 Collins, C., Ventrella, R., & Mitchell, B. J. (2021). Building a ciliated epithelium: Transcriptional regulation
417 and radial intercalation of multiciliated cells. *Curr Top Dev Biol, 145*, 3-39.
418 doi:10.1016/bs.ctdb.2020.08.001
419 Derderian, C., Canales, G. I., & Reiter, J. F. (2023). Seriously cilia: A tiny organelle illuminates evolution,
420 disease, and intercellular communication. *Dev Cell, 58*(15), 1333-1349.
421 doi:10.1016/j.devcel.2023.06.013
422 Eggenschwiler, J. T., & Anderson, K. V. (2007). Cilia and developmental signaling. *Annu Rev Cell Dev*
423 *Biol, 23*, 345-373. doi:10.1146/annurev.cellbio.23.090506.123249
424 Ferder, I. C., Fung, L., Ohguchi, Y., Zhang, X., Lassen, K. G., Capen, D., . . . Wang, N. (2019). Meiotic
425 gatekeeper STRA8 suppresses autophagy by repressing Nr1d1 expression during
426 spermatogenesis in mice. *PLoS Genet, 15*(5), e1008084. doi:10.1371/journal.pgen.1008084
427 Goetz, S. C., & Anderson, K. V. (2010). The primary cilium: a signalling centre during vertebrate
428 development. *Nat Rev Genet, 11*(5), 331-344. doi:10.1038/nrg2774
429 Holstein, A.-F., Schulze, W., & Davidoff, M. (2003). Understanding spermatogenesis is a prerequisite
430 for treatment. *Reproductive Biology and Endocrinology, 1*(1). doi:10.1186/1477-7827-1-107
431 Ishikawa, H., & Marshall, W. F. (2011). Ciliogenesis: building the cell's antenna. *Nat Rev Mol Cell Biol,*
432 *12*(4), 222-234. doi:10.1038/nrm3085
433 Jung, M., Wells, D., Rusch, J., Ahmad, S., Marchini, J., Myers, S. R., & Conrad, D. F. (2019). Unified single-
434 cell analysis of testis gene regulation and pathology in five mouse strains. *Elife, 8*.
435 doi:10.7554/eLife.43966
436 Kasahara, K., & Inagaki, M. (2021). Primary ciliary signaling: links with the cell cycle. *Trends Cell Biol,*
437 *31*(12), 954-964. doi:10.1016/j.tcb.2021.07.009
438 Kim, D., Langmead, B., & Salzberg, S. L. (2015). HISAT: a fast spliced aligner with low memory
439 requirements. *Nat Methods, 12*(4), 357-360. doi:10.1038/nmeth.3317
440 Kistler, W. S., Baas, D., Lemeille, S., Paschaki, M., Seguin-Estevez, Q., Barras, E., . . . Reith, W. (2015).
441 RFX2 Is a Major Transcriptional Regulator of Spermiogenesis. *PLoS Genet, 11*(7), e1005368.
442 doi:10.1371/journal.pgen.1005368

443 Lee, Y.-R., Khan, K., Armfield-Uhas, K., Srikanth, S., Thompson, N. A., Pardo, M., . . . Schwartz, C. E.
444 (2020). Mutations in FAM50A suggest that Armfield XLID syndrome is a spliceosomopathy.
445 *Nature Communications, 11*(1). doi:10.1038/s41467-020-17452-6
446 Lewis, M., & Stracker, T. H. (2021). Transcriptional regulation of multiciliated cell differentiation. *Semin*
447 *Cell Dev Biol, 110*, 51-60. doi:10.1016/j.semcdb.2020.04.007
448 Li, L., Tian, G., Peng, H., Meng, D., Wang, L., Hu, X., . . . Hu, Z. (2018). New class of transcription factors
449 controls flagellar assembly by recruiting RNA polymerase II in Chlamydomonas. *Proc Natl*
450 *Acad Sci U S A, 115*(17), 4435-4440. doi:10.1073/pnas.1719206115
451 Lin, Z., Hsu, P. J., Xing, X., Fang, J., Lu, Z., Zou, Q., . . . Tong, M. H. (2017). Mettl3-/Mettl14-mediated
452 mRNA N(6)-methyladenosine modulates murine spermatogenesis. *Cell Res, 27*(10), 1216-
453 1230. doi:10.1038/cr.2017.117
454 Lovera, M., & Lüders, J. (2021). The ciliary impact of nonciliary gene mutations. *Trends Cell Biol, 31*(11),
455 876-887. doi:10.1016/j.tcb.2021.06.001
456 Martianov, I., Fimia, G. M., Dierich, A., Parvinen, M., Sassone-Corsi, P., & Davidson, I. (2001). Late arrest
457 of spermiogenesis and germ cell apoptosis in mice lacking the TBP-like TLF/TRF2 gene. *Mol*
458 *Cell, 7*(3), 509-515. doi:10.1016/s1097-2765(01)00198-8
459 Martin-Tryon, E. L., & Harmer, S. L. (2008). XAP5 CIRCADIAN TIMEKEEPER coordinates light signals for
460 proper timing of photomorphogenesis and the circadian clock in Arabidopsis. *Plant Cell, 20*(5),
461 1244-1259. doi:10.1105/tpc.107.056655
462 Mazzarella, R., Pengue, G., Yoon, J., Jones, J., & Schlessinger, D. (1997). Differential expression of XAP5,
463 a candidate disease gene. *Genomics, 45*(1), 216-219. doi:10.1006/geno.1997.4912
464 Mitchell, D. R. (2017). Evolution of Cilia. *Cold Spring Harb Perspect Biol, 9*(1).
465 doi:10.1101/cshperspect.a028290
466 Nachury, M. V., & Mick, D. U. (2019). Establishing and regulating the composition of cilia for signal
467 transduction. *Nat Rev Mol Cell Biol*. doi:10.1038/s41580-019-0116-4
468 Nantel, F., Monaco, L., Foulkes, N. S., Masquilier, D., LeMeur, M., Henriksen, K., . . . Sassone-Corsi, P.
469 (1996). Spermiogenesis deficiency and germ-cell apoptosis in CREM-mutant mice. *Nature,*
470 *380*(6570), 159-162. doi:10.1038/380159a0
471 Nemajerova, A., Kramer, D., Siller, S. S., Herr, C., Shomroni, O., Pena, T., . . . Lize, M. (2016). TAp73 is a
472 central transcriptional regulator of airway multiciliogenesis. *Genes Dev, 30*(11), 1300-1312.
473 doi:10.1101/gad.279836.116
474 Oyama, Y., Miyata, H., Shimada, K., Larasati, T., Fujihara, Y., & Ikawa, M. (2022). TULP2 deletion mice
475 exhibit abnormal outer dense fiber structure and male infertility. *Reprod Med Biol, 21*(1),
476 e12467. doi:10.1002/rmb2.12467
477 Pertea, M., Pertea, G. M., Antonescu, C. M., Chang, T.-C., Mendell, J. T., & Salzberg, S. L. (2015).
478 StringTie enables improved reconstruction of a transcriptome from RNA-seq reads. *Nature*
479 *Biotechnology, 33*(3), 290-295. doi:10.1038/nbt.3122
480 Piasecki, B. P., Burghoorn, J., & Swoboda, P. (2010). Regulatory Factor X (RFX)-mediated transcriptional
481 rewiring of ciliary genes in animals. *Proc Natl Acad Sci U S A, 107*(29), 12969-12974.
482 doi:10.1073/pnas.0914241107
483 Qu, W., Yuan, S., Quan, C., Huang, Q., Zhou, Q., Yap, Y., . . . Zhang, Z. (2020). The essential role of

484 intraflagellar transport protein IFT81 in male mice spermiogenesis and fertility. *Am J Physiol*
485 *Cell Physiol, 318*(6), C1092-C1106. doi:10.1152/ajpcell.00450.2019
486 Reinholdt, L., Ashley, T., Schimenti, J., & Shima, N. (2004). Forward genetic screens for meiotic and
487 mitotic recombination-defective mutants in mice. *Methods Mol Biol, 262*, 87-107.
488 doi:10.1385/1-59259-761-0:087
489 Reiter, J. F., & Leroux, M. R. (2017). Genes and molecular pathways underpinning ciliopathies. *Nat Rev*
490 *Mol Cell Biol, 18*(9), 533-547. doi:10.1038/nrm.2017.60
491 Romanienko, P. J., & Camerini-Otero, R. D. (2000). The mouse Spo11 gene is required for meiotic
492 chromosome synapsis. *Mol Cell, 6*(5), 975-987. doi:10.1016/s1097-2765(00)00097-6
493 Santos, N., & Reiter, J. F. (2008). Building it up and taking it down: the regulation of vertebrate
494 ciliogenesis. *Dev Dyn, 237*(8), 1972-1981. doi:10.1002/dvdy.21540
495 Schartl, M., Schories, S., Wakamatsu, Y., Nagao, Y., Hashimoto, H., Bertin, C., . . . Herpin, A. (2018). Sox5
496 is involved in germ-cell regulation and sex determination in medaka following co-option of
497 nested transposable elements. *BMC Biol, 16*(1), 16. doi:10.1186/s12915-018-0485-8
498 Sedlacek, Z., Munstermann, E., Dhorne-Pollet, S., Otto, C., Bock, D., Schutz, G., & Poustka, A. (1999).
499 Human and mouse XAP-5 and XAP-5-like (X5L) genes: identification of an ancient functional
500 retroposon differentially expressed in testis. *Genomics, 61*(2), 125-132.
501 doi:10.1006/geno.1999.5931
502 Singla, V., & Reiter, J. F. (2006). The primary cilium as the cell's antenna: signaling at a sensory organelle.
503 *Science, 313*(5787), 629-633. doi:10.1126/science.1124534
504 Stubbs, J. L., Oishi, I., Izpisua Belmonte, J. C., & Kintner, C. (2008). The forkhead protein Foxj1 specifies
505 node-like cilia in Xenopus and zebrafish embryos. *Nat Genet, 40*(12), 1454-1460.
506 doi:10.1038/ng.267
507 Subramanian, A., Tamayo, P., Mootha, V. K., Mukherjee, S., Ebert, B. L., Gillette, M. A., . . . Mesirov, J. P.
508 (2005). Gene set enrichment analysis: A knowledge-based approach for interpreting genome-
509 wide expression profiles. *Proceedings of the National Academy of Sciences, 102*(43), 15545-
510 15550. doi:10.1073/pnas.0506580102
511 Swoboda, P., Adler, H. T., & Thomas, J. H. (2000). The RFX-type transcription factor DAF-19 regulates
512 sensory neuron cilium formation in C. elegans. *Mol Cell, 5*(3), 411-421. doi:10.1016/s1097-
513 2765(00)80436-0
514 Thomas, J., Morle, L., Soulavie, F., Laurencon, A., Sagnol, S., & Durand, B. (2010). Transcriptional control
515 of genes involved in ciliogenesis: a first step in making cilia. *Biol Cell, 102*(9), 499-513.
516 doi:10.1042/BC20100035
517 Thompson, N. A., Ranzani, M., van der Weyden, L., Iyer, V., Offord, V., Droop, A., . . . Adams, D. J. (2021).
518 Combinatorial CRISPR screen identifies fitness effects of gene paralogues. *Nature*
519 *Communications, 12*(1). doi:10.1038/s41467-021-21478-9
520 Vij, S., Rink, J. C., Ho, H. K., Babu, D., Eitel, M., Narasimhan, V., . . . Roy, S. (2012). Evolutionarily ancient
521 association of the FoxJ1 transcription factor with the motile ciliogenic program. *PLoS Genet,*
522 *8*(11), e1003019. doi:10.1371/journal.pgen.1003019
523 Weidemann, M., Schuster-Gossler, K., Stauber, M., Wrede, C., Hegermann, J., Ott, T., . . . Gossler, A.
524 (2016). CFAP157 is a murine downstream effector of FOXJ1 that is specifically required for

525 flagellum morphogenesis and sperm motility. *Development, 143*(24), 4736-4748.
526 doi:10.1242/dev.139626
527 Wu, Y., Hu, X., Li, Z., Wang, M., Li, S., Wang, X., . . . Han, C. (2016). Transcription Factor RFX2 Is a Key
528 Regulator of Mouse Spermiogenesis. *Sci Rep, 6*, 20435. doi:10.1038/srep20435
529 Yu, X., Ng, C. P., Habacher, H., & Roy, S. (2008). Foxj1 transcription factors are master regulators of the
530 motile ciliogenic program. *Nat Genet, 40*(12), 1445-1453. doi:10.1038/ng.263
531 Zhang, A., Skaar, D. A., Li, Y., Huang, D., Price, T. M., Murphy, S. K., & Jirtle, R. L. (2011). Novel
532 retrotransposed imprinted locus identified at human 6p25. *Nucleic Acids Res, 39*(13), 5388-
533 5400. doi:10.1093/nar/gkr108
534 Zhang, D., Xie, D., Lin, X., Ma, L., Chen, J., Zhang, D., . . . Han, C. (2018). The transcription factor SOX30
535 is a key regulator of mouse spermiogenesis. *Development, 145*(11). doi:10.1242/dev.164723
536 Zheng, M., Chen, X., Cui, Y., Li, W., Dai, H., Yue, Q., . . . Zhu, H. (2021). TULP2, a New RNA-Binding
537 Protein, Is Required for Mouse Spermatid Differentiation and Male Fertility. *Front Cell Dev Biol,*
538 *9*, 623738. doi:10.3389/fcell.2021.623738
539 Zhou, H., Grubisic, I., Zheng, K., He, Y., Wang, P. J., Kaplan, T., & Tjian, R. (2013). Taf7l cooperates with
540 Trf2 to regulate spermiogenesis. *Proc Natl Acad Sci U S A, 110*(42), 16886-16891.
541 doi:10.1073/pnas.1317034110

542

Figures

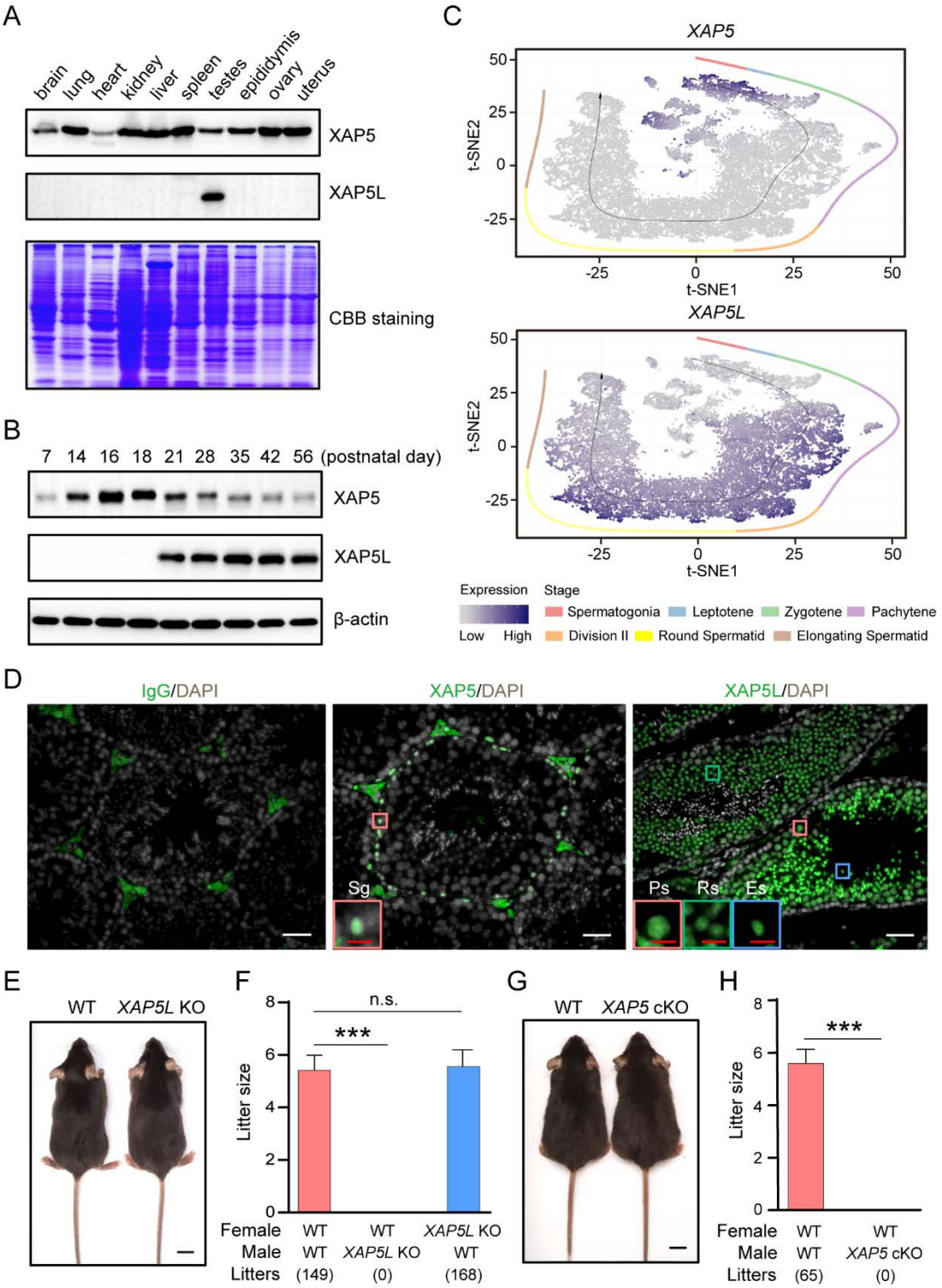

Figure 1. Loss of XAP5 and XAP5L proteins results in male mice infertility.

(A) Detection of XAP5/XAP5L protein in different tissues of adult mice by Western blot analysis. **(B)** Expression of XAP5/XAP5L protein during postnatal testicular development. β-actin was used as control. **(C)** t-SNE plots displaying *XAP5*/*XAP5L* gene expression levels in individual cell types of mouse testis visualized using published single-cell data(Jung et al., 2019). Black arrow represents the developmental pseudotime corresponding to the developmental ordering of each cell progressing through spermatogenesis. Dot color intensity represents the expression level. Cells from different stages are color-coded. **(D)** Immunofluorescence staining of XAP5/XAP5L in adult WT testis. Representative spermatogonium (Sg), round spermatid (Rs) and elongating spermatid (Es) are indicated. Scale bars: 20 μm (white), 5 μm (red). **(E)** Similar development between WT and *XAP5L* KO mice. Scale bar: 1 cm. **(F)** Average litter size of pups obtained by fertility test. Each male was caged with two females for 2 months, 5 males were used for each genotype. ***$P < 0.001$, n.s. stands for not significant. **(G)** Similar appearance of WT and *XAP5* cKO mice. Scale bar: 1 cm. **(H)** Average litter size of pups obtained by fertility test. Each male was caged with two WT females for 2 months, 4 males were used for each genotype. ***$P < 0.001$. Error bars depict means ± SEM. All *P*-values were calculated using an unpaired, two-tailed Student's t-test.

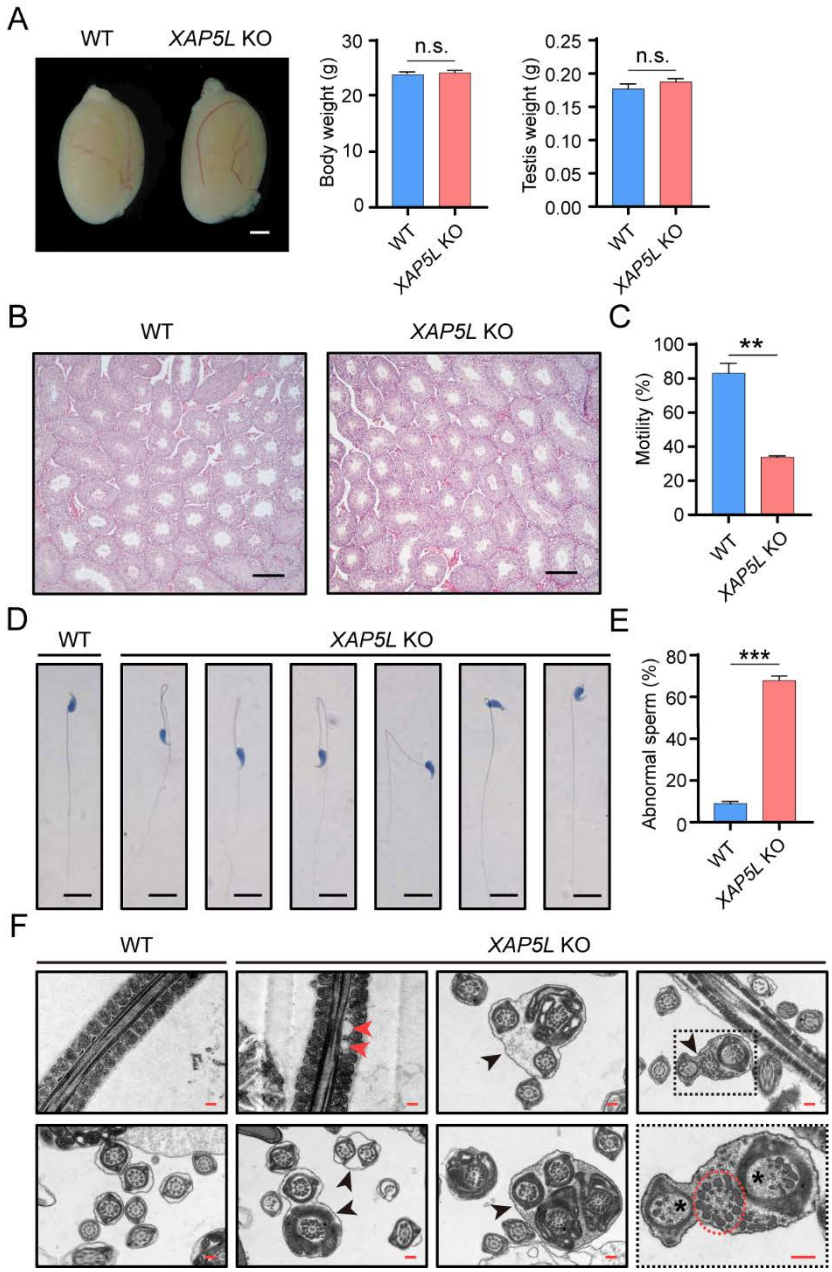

Figure 2. XAP5L is required for normal sperm formation.

(A) Similar gross testes morphology, body weight and testis weight between WT and *XAP5L* KO mice. Scale bar: 1 mm. n = 6, n.s. stands for not significant. **(B)** H&E staining showing similar histological structure of the testes from WT and *XAP5L* KO mice. Scale bars: 100 μm. **(C)** Significantly reduced sperm total motility of *XAP5L* KO mice. n = 3,

$P < 0.01$. **(D) H&E staining showing the morphology of sperm in WT and *XAP5L* KO mice. Scale bars: 10 μm. **(E)** Significantly increased abnormal sperm in *XAP5L* KO mice. n = 6, ***$P < 0.001$. **(F)** Electron microscopic analysis displaying ultrastructural defects in *XAP5L* KO sperm flagella, including cytoplasmic vacuoles enveloping mitochondrial sheath (as shown by red arrowheads), a complete lack of mitochondrial sheath (as shown by red dotted circle), two or more cross-sections of the same sperm flagellum enclosed within one cell membrane (as shown by black arrowheads), partially formed outer dense fibers, and the axonemal microtubules (as indicated by asterisks). Scale bars: 2 μm. Error bars depict means ± SEM. All *P*-values were calculated using an unpaired, two-tailed Student's t-test.

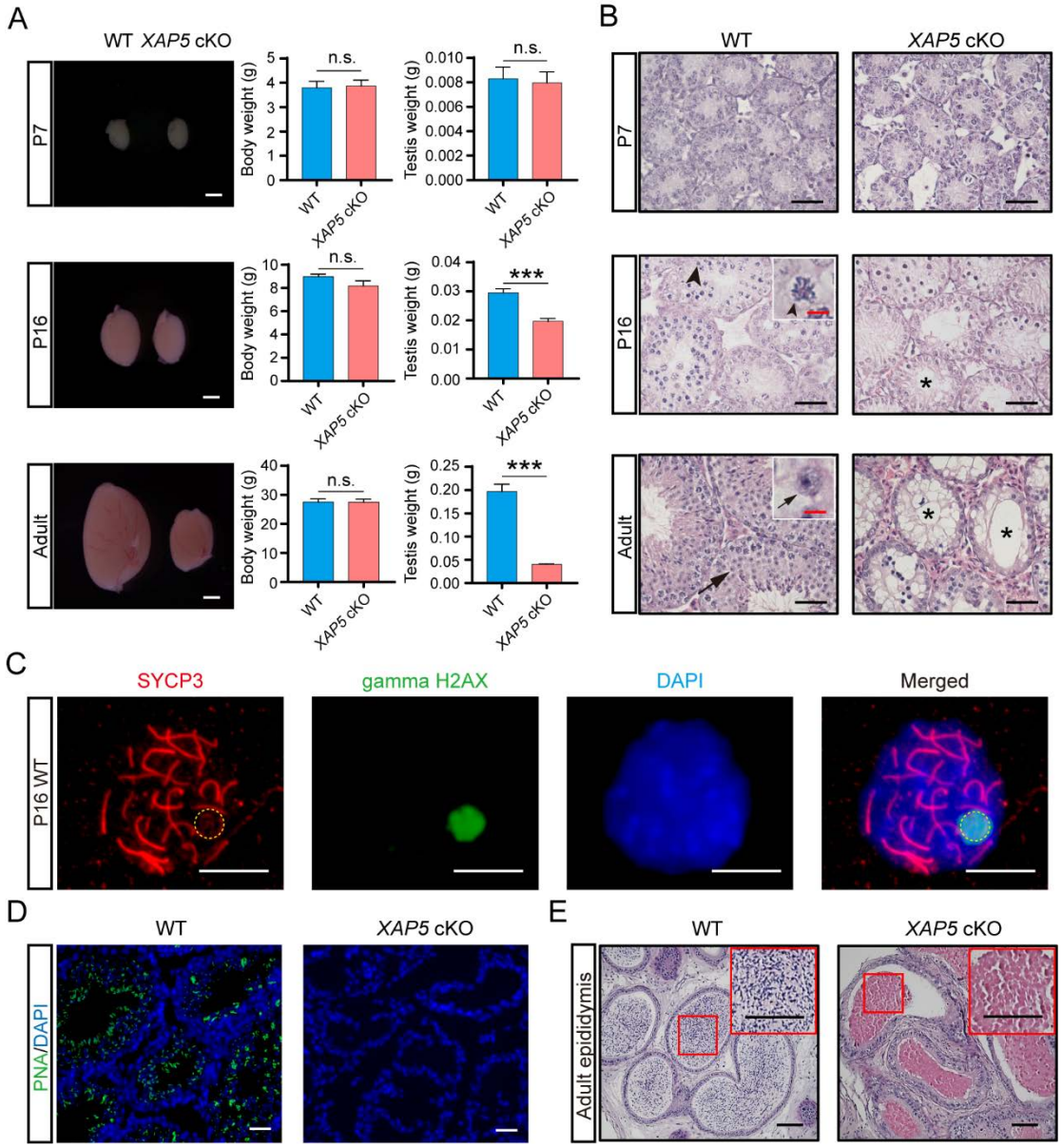

Figure 3. Ablation of XAP5 in germ cells results in arrested spermatogenesis and absence of sperm.

(A) Testes sizes, body weight and testis weight from WT and *XAP5* cKO mice at various ages were evaluated. Similar body weight was observed between WT and *XAP5* cKO mice. No significant difference in size and weight was detected between WT and *XAP5* cKO testes until P16. Scale bars: 1 mm. n = 5, ***$P < 0.001$, n.s. stands for not significant. **(B)**

Histology of testes from WT and *XAP5* cKO mice at various ages were evaluated by H&E staining. No pachytene spermatocytes were found, and many vacuolated tubules were observed in *XAP5* cKO testis since P16. Black arrowheads indicate pachytene spermatocytes; black arrows indicate round spermatids. Vacuolated seminiferous tubules are indicated by asterisks. Scale bars: 20 μm (black), 2.5 μm (red). **(C)** Chromosome spreads staining showing pachytene spermatocytes from P16 WT male mouse. Yellow dotted circle indicates the XY body. Scale bars: 10 μm. **(D)** Immunofluorescence staining of PNA in adult testes indicating the absence of spermatids in *XAP5* cKO mice. Scale bars: 20 μm. **(E)** H&E staining of adult epididymis displaying absence of sperm in *XAP5* cKO mice. Scale bars: 50 μm. Error bars depict means ± SEM. All *P*-values were calculated using an unpaired, two-tailed Student's t-test.

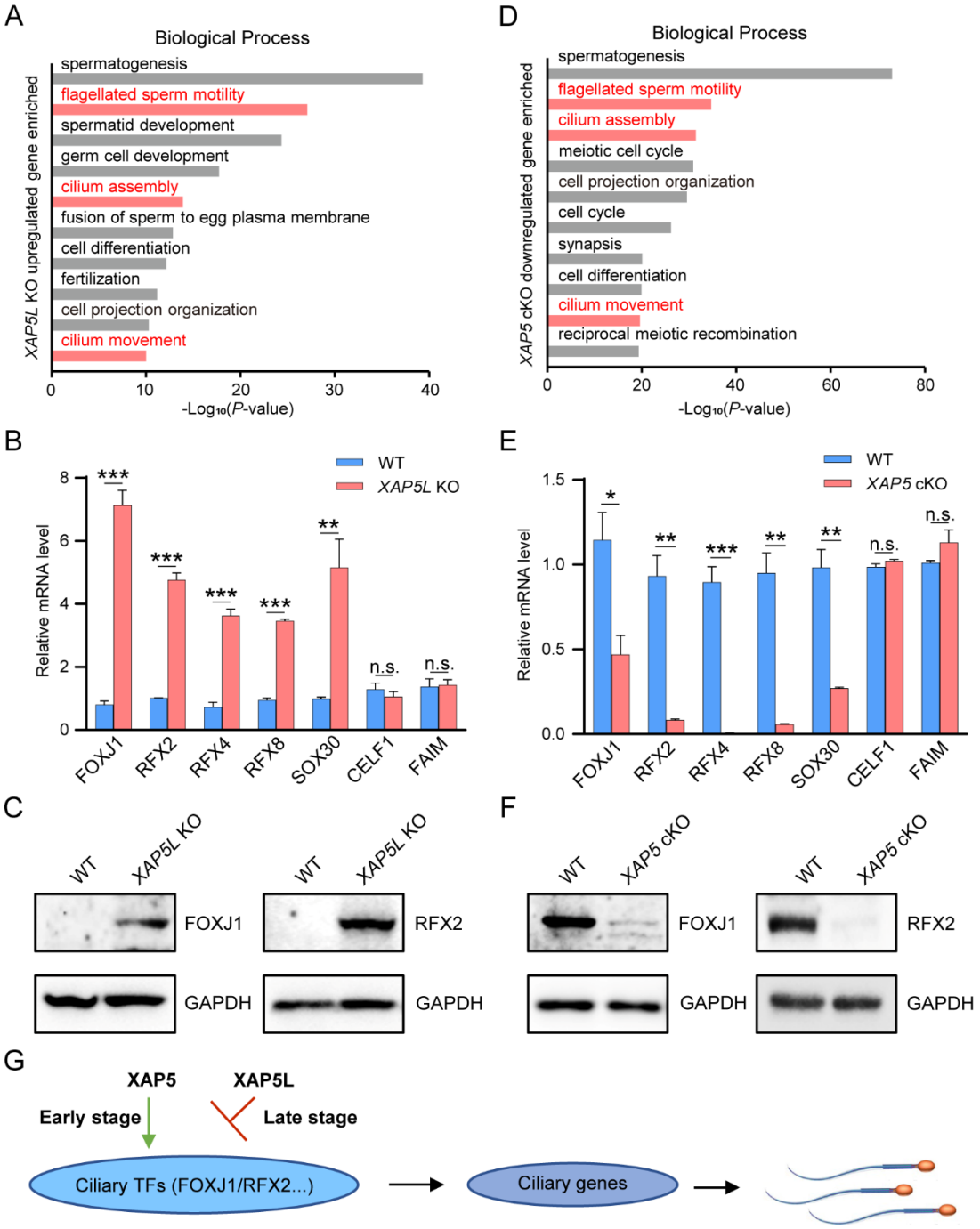

Figure 4. Aberrant ciliogenic and spermatogenic gene expression in *XAP5L* KO and *XAP5* cKO male germ cells.

(A) Gene ontology analysis showing top ten biological process terms significantly enriched among upregulated genes in *XAP5L* KO sperm. **(B)** Real-time PCR validation of genes

involved in ciliogenesis and spermatogenesis. n = 3, $^{**}P < 0.01$, $^{***}P < 0.001$, n.s. stands for not significant. **(C)** Detection of FOXJ1 and RFX2 in mature sperm of WT and *XAP5L* KO mice by Western blot analysis. GAPDH was used as a control. **(D)** Gene ontology analysis showing top ten biological process terms significantly enriched among downregulated genes in P16 *XAP5* cKO testes. **(E)** Real-time PCR validation of genes involved in ciliogenesis and spermatogenesis. n = 3, $^{*}P < 0.05$, $^{**}P < 0.01$, $^{***}P < 0.001$, n.s. stands for not significant. **(F)** Detection of FOXJ1 and RFX2 in P16 testes of WT and *XAP5* cKO mice by Western blot analysis. GAPDH was used as a control. **(G)** A model on the involvement of XAP5 and XAP5L in the regulation of ciliogenesis during spermatogenesis. Error bars depict means ± SEM. All *P*-values were calculated using an unpaired, two-tailed Student's t-test.

Supplementary Figures

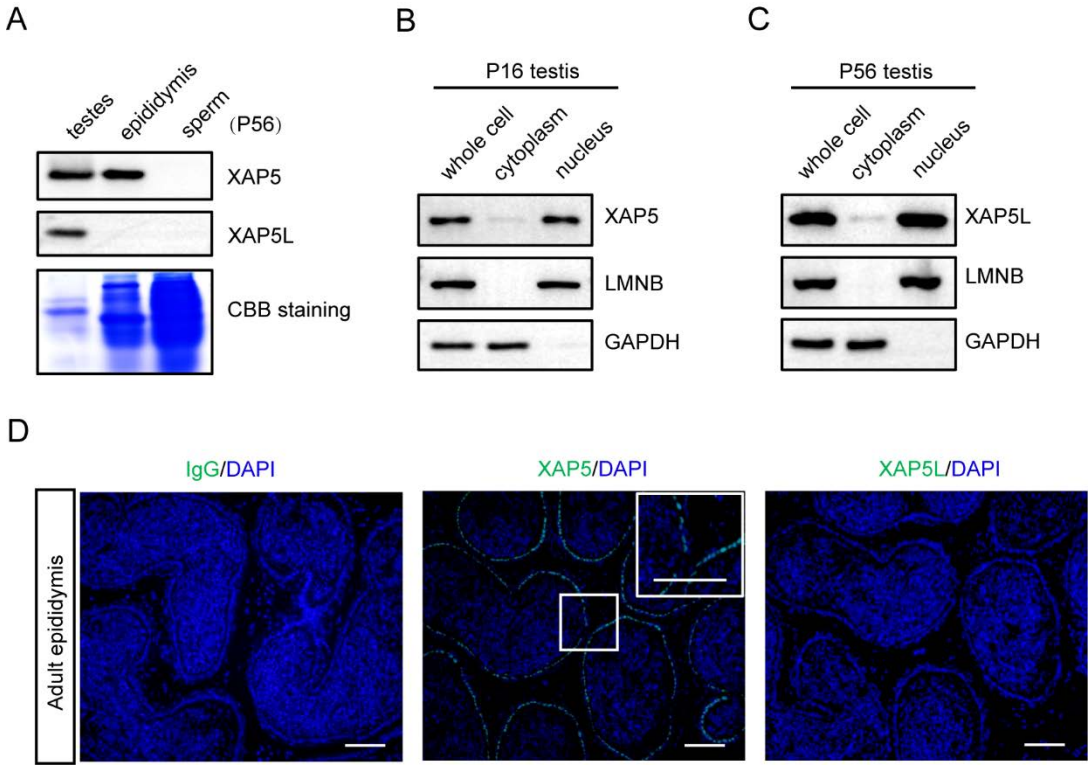

Figure S1. Localization of XAP5/XAP5L in testicular cells.

(A) Western blot analysis showing no localization of XAP5/XAP5L in mature sperm. Western blot analysis showing the subcellular localization of endogenous XAP5 (**B**) and XAP5L (**C**). LMNB used as a nuclear protein marker, GAPDH used as a cytoplasmic protein marker. **(D)** Immunofluorescence staining of XAP5/XAP5L in adult epididymis. Scale bars: 50 μm.

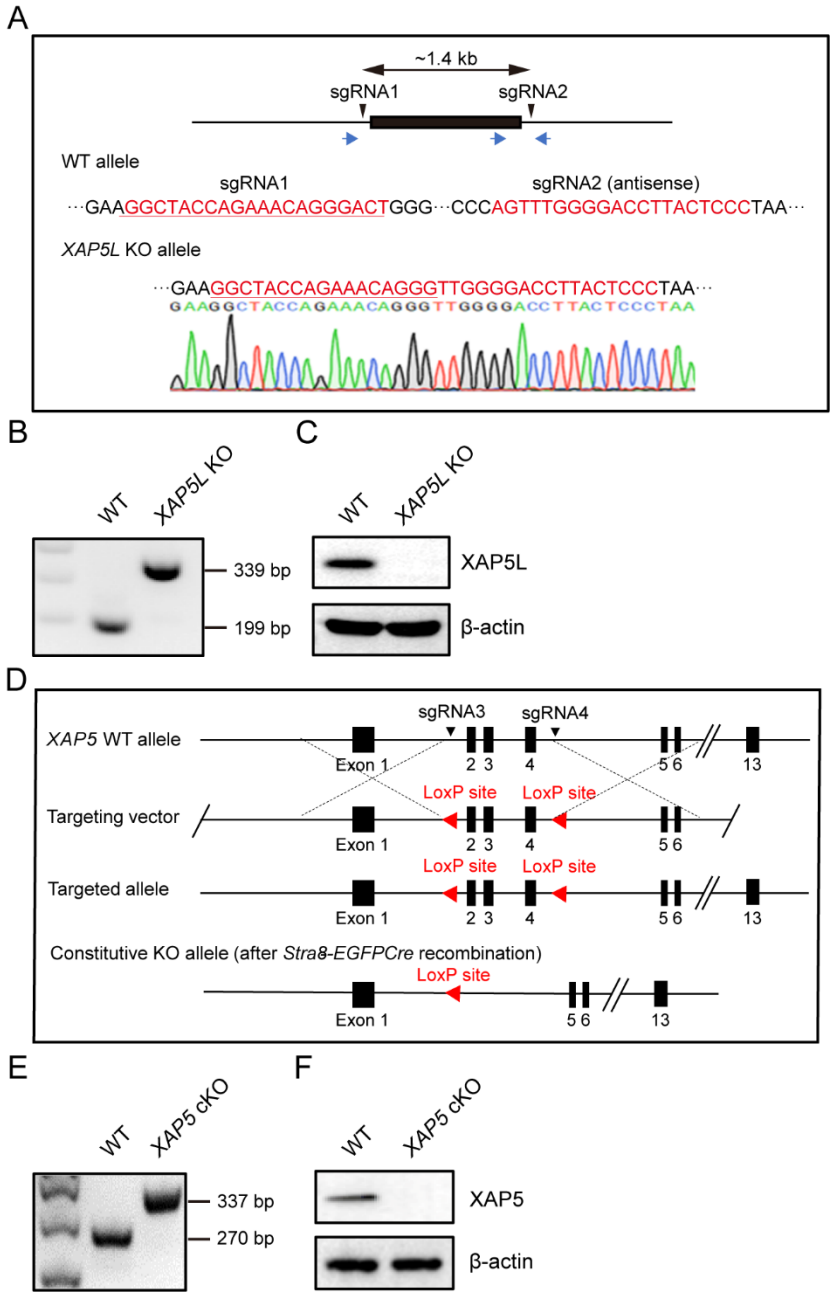

Figure S2. Generation of *XAP5L* KO and *XAP5* cKO mice.

(A) Schematic illustration of the targeting strategy for generating a *XAP5L* knockout mouse line using CRISPR-Cas9 system. Upper panel showing genomic structure of the *XAP5L* gene. The location of two sgRNAs (sgRNA1 and sgRNA2) used and three primers (blue arrows) for genome PCR are indicated. Lower panel displaying nucleotide sequence of WT

allele in the vicinity of two sgRNAs (red color) and the corresponding sequence of the *XAP5L* homozygous mutant (KO) allele. The deletion of *XAP5L* gene was verified by Sanger sequencing. **(B)** Genome PCR analysis in WT and *XAP5L* KO mice. **(C)** Detection of XAP5L in adult testes extracts of WT and *XAP5L* KO mice by Western blot analysis. β-actin was used as a control. **(D)** Schematic illustration of the targeting strategy for generating *XAP5* cKO mice. The location of LoxP sites inserted and the primers (blue arrow) used for genome PCR are indicated. **(E)** Genome PCR analysis in WT and *XAP5* cKO mice. **(F)** Detection of XAP5 in testes extracts of WT and *XAP5* cKO mice by Western blot analysis. β-actin was used as a control.

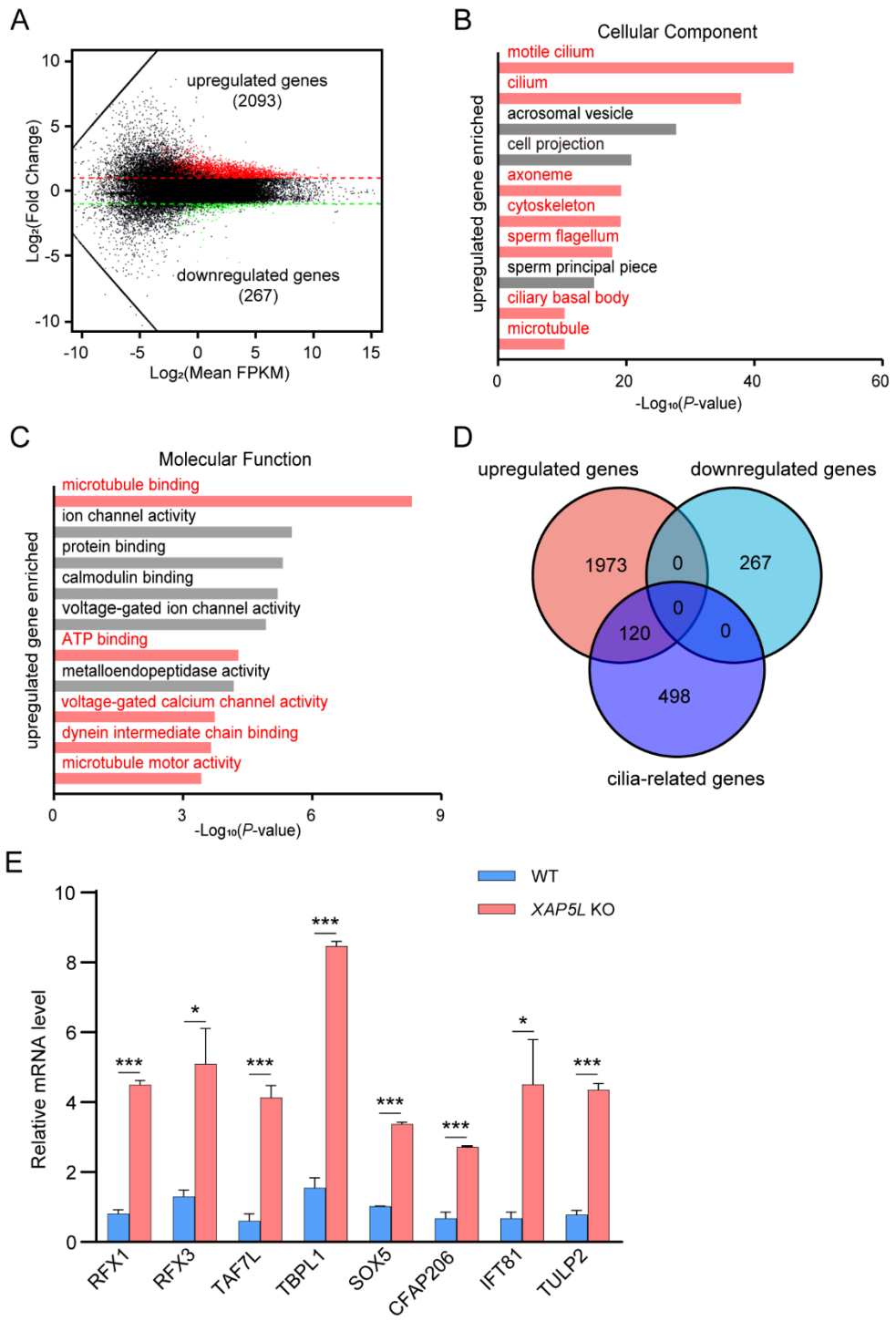

Figure S3. XAP5L-mediated regulation of ciliary gene expression during mouse spermatogenesis.

(A) MA plot showing the numbers of differentially expressed genes in *XAP5L* KO sperm.

Gene ontology analysis showing top ten cellular component (**B**) and molecular function (**C**) terms significantly enriched among upregulated genes in *XAP5L* KO sperm. **(D)** Venn diagram representing total genes upregulated/downregulated by at least twofold in *XAP5L* KO sperm and published cilia-related genes(Nemajerova et al., 2016). **(E)** Real-time PCR validation of genes involved in ciliogenesis and spermatogenesis. n = 3, *$P < 0.05$, ***$P < 0.001$. Error bars depict means ± SEM. All *P*-values were calculated using an unpaired, two-tailed Student's t-test.

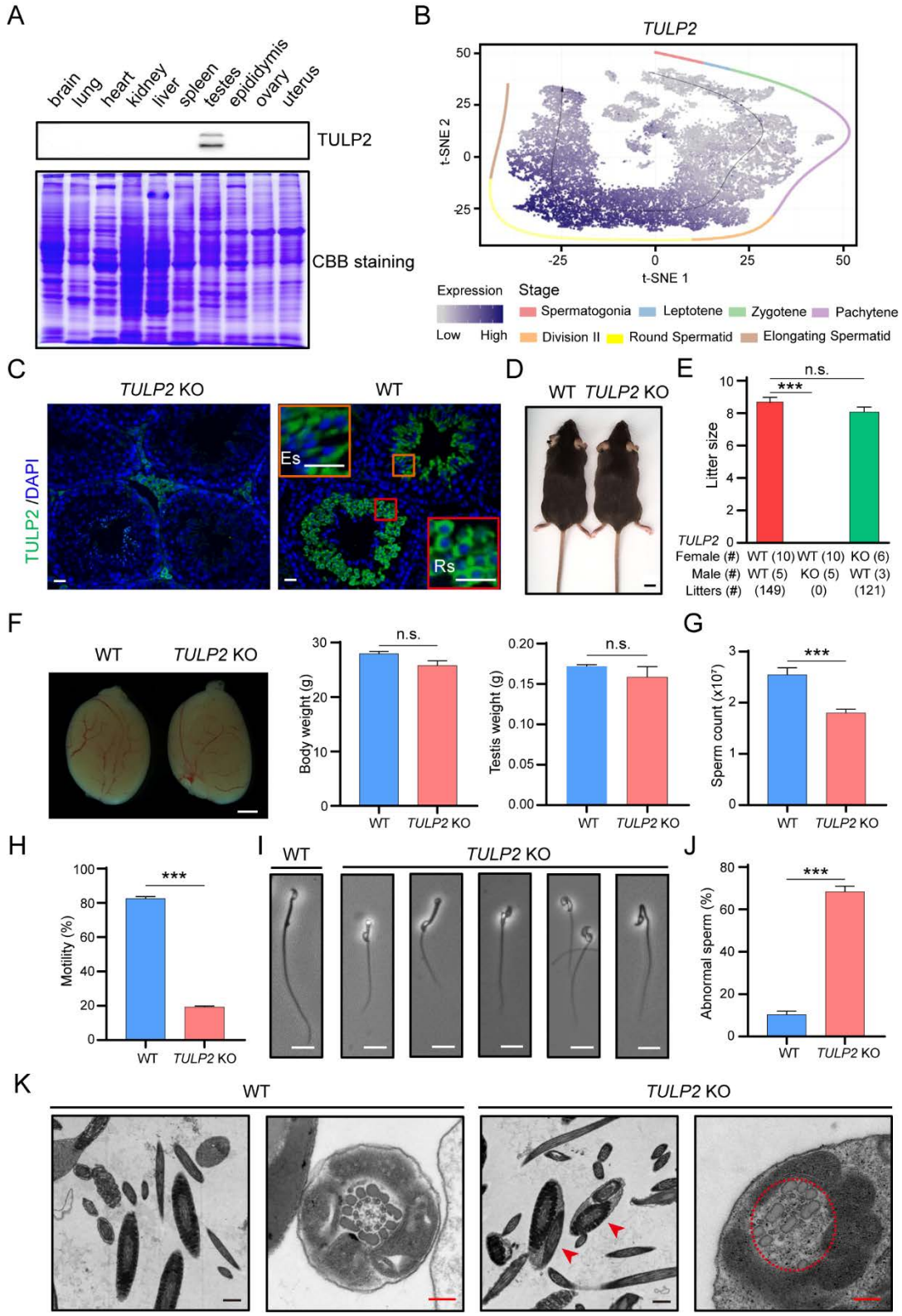

Figure S4. *TULP2* KO male mice were infertile due to malformation of sperm.

(A) Detection of TULP2 protein in different tissues of adult mice by Western blot analysis.

(B) t-SNE plot displaying *TULP2* gene expression pattern during spermatogenesis visualized using published single-cell data(Jung et al., 2019). Black arrow represents the developmental pseudotime corresponding to the developmental ordering of each cell progressing through spermatogenesis. Dot color intensity represents the expression level. Cells from different stages are color-coded. **(C)** Immunofluorescence staining showing TULP2 expression in the cytoplasm of round spermatids (Rs) and elongating spermatids (Es). Scale bars: 5 μm. **(D)** Similar development of adult WT and *TULP2* KO mice. Scale bar: 1 cm. **(E)** Average litter size of pups obtained by fertility test. Each male was caged with two females for 2 months. ***$P < 0.001$, n.s. stands for not significant. **(F)** Similar gross testes morphology, body weight and testis weight between WT and *TULP2* KO mice. Scale bar: 1 mm. n = 4, n.s. stands for not significant. **(G)** Significantly reduced caudal epididymal sperm counts in *TULP2* KO mice compared with WT males. n = 7, ***$P < 0.001$. **(H)** Significantly reduced sperm total motility of *TULP2* KO mice. n = 3, ***$P < 0.001$. Significantly increased abnormal sperm in *TULP2* KO mice (**I** and **J**). Scale bars: 10 μm. n = 3, ***$P < 0.001$. **(K)** Electron microscopic analysis displaying ultrastructural defects in *TULP2* KO sperm flagella, including two cross-sections of the same sperm flagellum enclosed within one cell membrane (as shown by red arrowheads), disorganized outer dense fibers and the axonemal microtubules (as shown by red dotted circle). Scale bars: 8 μm (black), 2 μm (red). Error bars depict means ± SEM. All *P*-values were calculated using an unpaired, two-tailed Student's t-test.

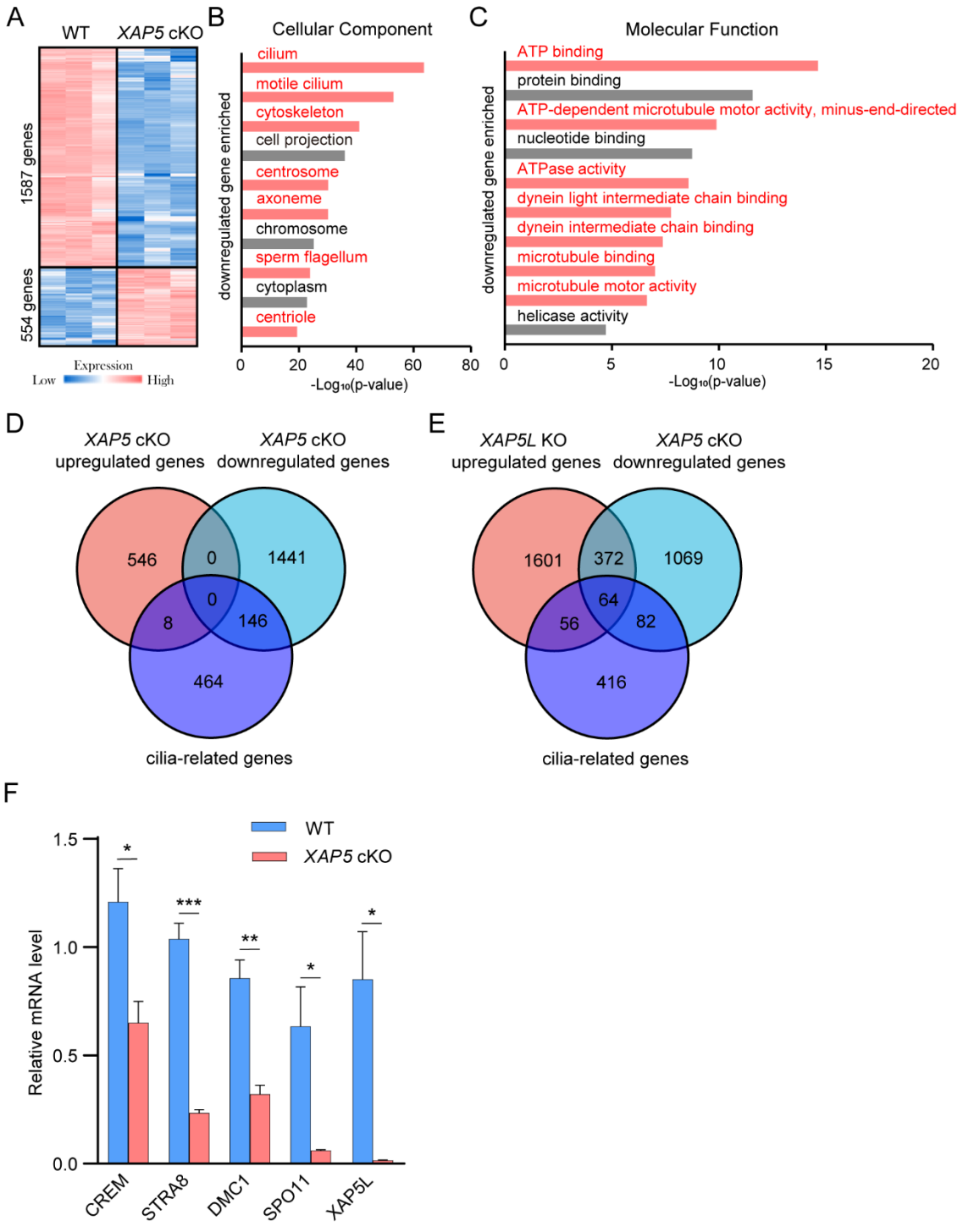

Figure S5. XAP5-mediated regulation of ciliary gene expression during mouse spermatogenesis.

(A) Heat map showing variably expressed genes in P16 *XAP5* cKO testes. Number of

related genes was indicated. Gene ontology analysis showing top ten cellular component (**B**) and molecular function (**C**) terms significantly enriched among downregulated genes in *XAP5* cKO testes. **(D)** Venn diagram representing total genes upregulated/downregulated in *XAP5* cKO testes and published cilia-related genes(Nemajerova et al., 2016). **(E)** Venn diagram representing total genes downregulated in *XAP5* cKO testes, upregulated in *XAP5L* KO sperm by at least twofold and published cilia-related genes(Nemajerova et al., 2016). **(F)** Real-time PCR validation of genes involved in ciliogenesis and spermatogenesis. n = 3, *$P < 0.05$, **$P < 0.01$, ***$P < 0.001$. Error bars depict means ± SEM. All P-values were calculated using an unpaired, two-tailed Student's t-test.

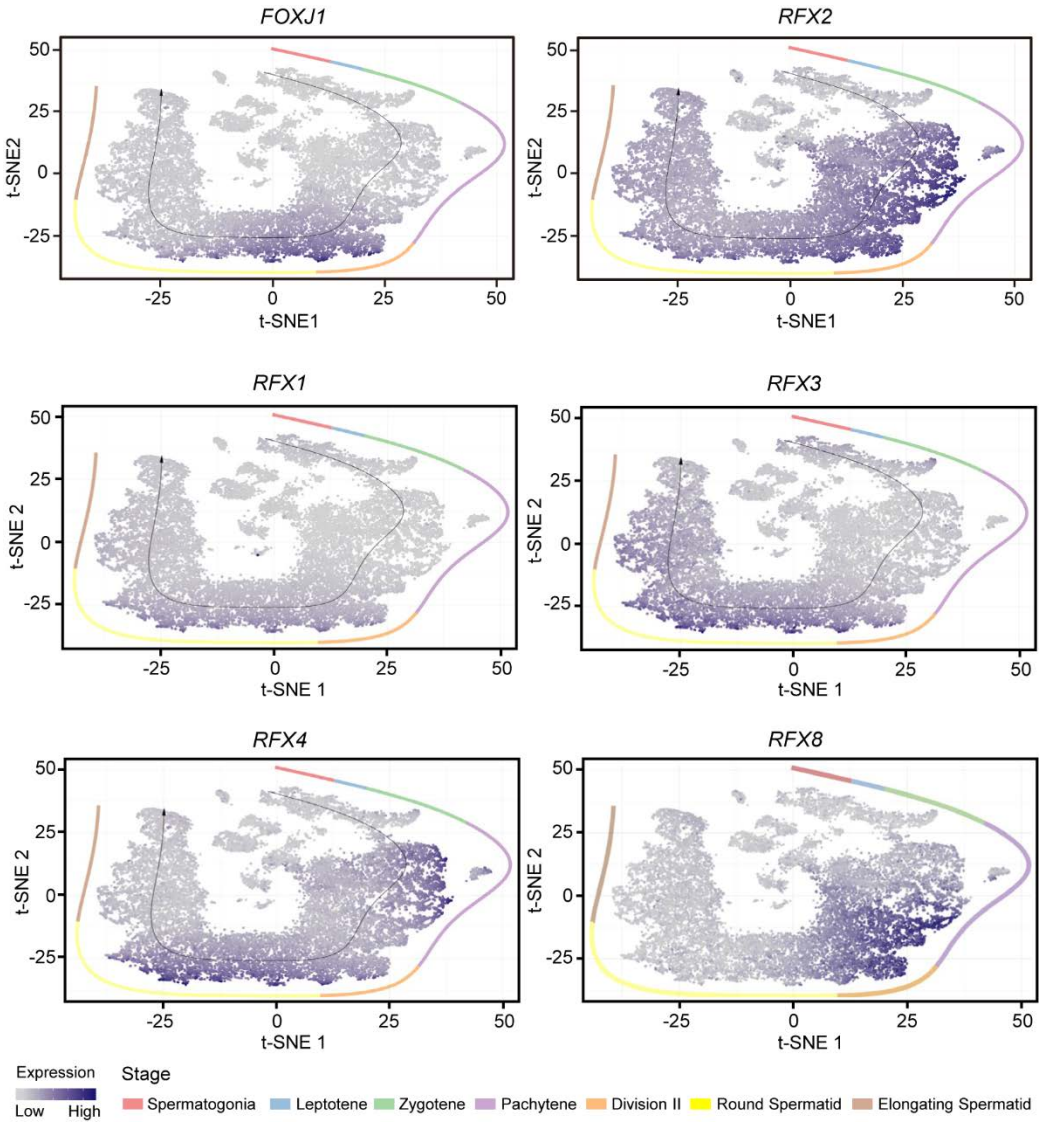

Figure S6. t-SNE plots displaying expression patterns of *FOXJ1* and *RFX* families in individual cell types of mouse testes.

The black arrow represents the developmental pseudotime corresponding to the developmental ordering of each cell progressing through spermatogenesis. Dot color intensity represents the relative expression level. Cells from different stages are color-coded. The gene expression was visualized using the published single-cell data(Jung et al., 2019).